Structure, vibrational and magnetic characteristics of LiYbX2O8 (X = W, Mo) single-crystals

Pascale Armand, Dominique Granier, Corine Reibel, Léa Daenens, Monique Tillard

Structure, vibrational and magnetic characteristics of $LiYbX_2O_8$ (X= W, Mo) single-crystals

Pascale Armand, Dominique Granier, Corine Reibel, Léa Daenens, Monique Tillard

PII: S0925-8388(21)02483-X

DOI: https://doi.org/10.1016/j.jallcom.2021.161074

Reference: JALCOM161074

To appear in: *Journal of Alloys and Compounds*

Received date: 28 May 2021
Accepted date: 4 July 2021

Please cite this article as: Pascale Armand, Dominique Granier, Corine Reibel, Léa Daenens and Monique Tillard, Structure, vibrational and magnetic characteristics of $LiYbX_2O_8$ (X= W, Mo) single-crystals, *Journal of Alloys and Compounds,* (2021) doi:https://doi.org/10.1016/j.jallcom.2021.161074

Structure, vibrational and magnetic characteristics of $LiYbX_2O_8$ (X = W, Mo) single-crystals

Pascale Armand*, Dominique Granier, Corine Reibel,

Léa Daenens, Monique Tillard

ICGM, Univ. Montpellier, CNRS, ENSCM, Montpellier, France

ORCID: P. Armand 0000-0001-8921-5427; M. Tillard 0000-0002-0609-7224

*Corresponding author: pascale.armand@umontpellier.fr,

ICGM, Univ. Montpellier, CC 1504, 34095 Montpellier Cedex 5, France

Abstract

Crystals of the Yb-containing double tungstate and double molybdate $LiYbX_2O_8$ (X = W, Mo) have been spontaneously grown by a high-temperature flux technique. Their structure has been determined from single-crystal X-ray diffraction at room temperature. $LiYbW_2O_8$ crystallizes in the monoclinic $P2/n$ space group (No. 13), with unit cell parameters a = 4.9910(2), b = 5.7964(2), c = 9.8886(4) Å, β = 93.353(1) °. $LiYbMo_2O_8$ displays the tetragonal symmetry and is described in the noncentrosymmetric $I\bar{4}$ space group (No. 82) with $a = b$ = 5.1149(1), c = 11.0919(4) Å. Structural features such as coordination numbers around the atoms and ordered/disordered arrangement of the Yb^{3+} and Li^{+} cations explain the differences between these compounds whose vibrational and magnetic properties have also been studied.

Keywords

A. oxide material; B. crystal growth; C. crystal structure; D. magnetic measurements; D. X-ray diffraction; D. inelastic light scattering.

1. INTRODUCTION

Compounds having the general stoichiometric formula ATX_2O_8, with a monovalent metal *A*, a trivalent metal *T*, and a main element *X* = W^{VI} or Mo^{VI}, exist for numerous chemical combinations with a wide variety of structural forms [1-6]. The presence of Li as the *A* component makes the lithiated members of this family potential candidates as anode materials in lithium-ion batteries [7,8]. The double molybdate and double tungstate families with trivalent lanthanide (*Ln*) are attracting materials for industrial applications with multifunctional physical properties depending on both the rare-earth element and the crystal structure [6-9]. For example, some are suitable for laser operation and/or as *Ln*-doped hosts in the field of fluorescence, while others exhibit ferroelectricity and ferroelasticity phenomena [1,2,6,9]. The trivalent rare-earth oxides with 4*f* electrons are also remarkable for another important physical property which is their magnetic response. $LiFe(MoO_4)_2$, a member of the double molybdate family, undergoes an antiferromagnetic transition while the multiferroic double tungstate $LiFe(WO_4)_2$ exhibits two successive magnetic transitions [10,11]. It is thus important to characterize the magnetic properties of other *Ln*-based double molybdates and tungstates such as $LiYbX_2O_8$ (*X* = W, Mo).

A cationic Yb^{3+}/Li^{+} disorder over two atomic sites was previously evidenced for the double molybdate $LiYbMo_2O_8$ reported with a tetragonal Scheelite-type structure, and a correlation was proposed between its properties and the random distribution of cations [1, 2]. Besides, an ordered arrangement of the cations was found in the double tungstate β-$LiYbW_2O_8$ characterized with a Wolframite-based monoclinic structure [4,5] from powder diffraction data.

This paper summarizes our latest results relative to the flux-grown synthesis, the X-ray single-crystal structure determination as well as the study of the vibrational and magnetic properties

of the lithium ytterbium double molybdate and double tungstate materials, $LiYbMo_2O_8$ and $LiYbW_2O_8$.

2. EXPERIMENTAL SECTION

Crystals were obtained using the high-temperature flux method described elsewhere [12]. For the present study, the mixtures Li_2O-$3MoO_3$ and Li_2O-$2WO_3$ chosen as fluxes were previously prepared from alkali carbonate Li_2CO_3 and MoO_3/WO_3 powders *via* a solid-state reaction in the air at 500 °C for two weeks. All the reagents are commercial Alfa Aesar products of the analytical-and-research-grade with purity ≥ 99%. The selected flux and Yb_2O_3 taken in a 90/10 weight ratio were thoroughly mixed and a total amount of 20 g, placed in a Pt crucible, was heated in air at 970 °C for 5 h to obtain a homogeneous melt. Then, a slow decrease in temperature to 600 °C was programmed at a rate of 0.9 °/h, and cooling was continued at 200 °/h from 600 °C to room temperature. The numerous crystals formed spontaneously were isolated by the dissolution of the flux mixture in water. The as-grown crystals were directly used for characterization through classical methods and more precision on the conditions for spectroscopy or X-ray diffraction experiments can be found in our previous paper [12].

Crystals for X-ray diffraction experiments have been selected under a stereomicroscope equipped with a polarizing filter. The diffracted intensities were measured at room temperature (298 K) on a 4-circle diffractometer using the Mo Kα radiation λ = 0.71073 Å, Bruker D8 Venture (Incoatec micro source, Photon II CPAD detector) or Xcalibur CCD (Oxford Diffraction). They were processed with the appropriate software suite, either Apex [13] or CrysAlis [14]. The structures were solved and refined using the SHELX programs [15-16] and all atoms were considered with anisotropic displacement parameters in the final

full-matrix least-squares refinements on F^2. The chemical compositions were checked via classical EDX measurements that also proved the good homogeneity of the crystals.

Magnetic susceptibility and ZFC-FC magnetization cycle measurements (ZFC = zero-field cooled, FC = field cooled) were performed using a squid magnetometer Quantum Design MPMS 7XL, allowing to explore the temperature range 1.8 - 400 K with magnetic fields varying from −7 to 7 T (7×10^4 Oe). Several crystals with a sub-millimeter size were weighted and blocked in a gelatin capsule and then inserted in a plastic straw. The total mass of crystals was 4.15 mg for $LiYbMo_2O_8$ and 22.3 mg of $LiYbW_2O_8$. No variation was observed between the data collected after cooling the sample in a magnetic field (FC) and the data collected after cooling in a zero field (ZFC). The magnetic susceptibility was corrected from both the contribution of the capsule and the diamagnetic contribution of the elements with χ_{dia} estimated at $-3.38.10^{-4}$ emu/mol and $-2.50.10^{-4}$ emu/mol, respectively for $LiYbW_2O_8$ and $LiYbMo_2O_8$.

3. RESULTS AND DISCUSSION

3.1 Flux-grown crystals

As-grown crystals of sub-millimeter size were obtained *via* spontaneous nucleation from the high-temperature flux method. The crystals grown in the experiment with Yb_2O_3/Li_2O-$3MoO_3$ are transparent, colorless, and have faceted 3D-like shapes. The flux-growth experiment conducted with Yb_2O_3/Li_2O-$2WO_3$ also provided transparent and colorless crystals but as thin plates. The as-grown crystals were directly recovered for characterization without being subjected to further annealing treatment.

3.2 Structure solution and refinement

3.2.1. Structure of the double tungstate $LiYbW_2O_8$

A thin and colorless platelet was chosen among flat crystals displaying a clear trend to twinning. The recorded data were indexed in a monoclinic cell of parameters a = 4.9910(2), b = 5.7964(2), c = 9.8886(4) Å, β = 93.353(1) °. The centrosymmetric space group $P2/n$ (n° 13) was suggested by the statistics and the extinction conditions. A Fourier difference allowed us to find the position of Li to add to the initial model comprising four oxygen and two heavy-atoms. The free refinement of occupation factors agrees with a complete filling of the atom sites. The final refinement to R1 = 2.56% was performed with a set of reflections limited to theta angles less than 27 ° because both the residual density peaks, very close to the heavy atoms in the last Fourier difference, and the slight splitting of the diffraction spots at high angles suggest multiple crystals. The main crystal information and refinement data are summarized in Table 1.

Table 1. Room temperature crystal data and structure refinement parameters.

	$LiYbW_2O_8$	**$LiYbMo_2O_8$**
CSD number	2086021	2086022
M, Z	675.68, 2	499.86, 2
Calc. density (Mg/m^3)	7.857	5.721
System, space group	Monoclinic, $P2/n$ (13)	Tetragonal $I\bar{4}$ (82)
Unit cell dimensions (Å, °)	a = 4.9910(2), b = 5.7964(2)	$a = b$ = 5.1150(1),
	c = 9.8886(4), β = 93.353(1)	c = 11.0919(4)
Volume ($Å^3$)	285.586(19)	290.197(15)
Abs. coefficient (mm^{-1})	56.419	20.236
Crystal size (mm)	0.044 × 0.035 × 0.020	0.232 × 0.097 × 0.085
Diffractometer	Bruker D8 Venture	Xcalibur CCD
Collected / independent refls.	2242 / 623 [R_{int} = 0.0359]	2468 / 429 [R_{int} = 0.0681]

Final R indices [I>2σ(I)]	R1 = 0.0256, wR2 = 0.0651	R1 = 0.0273, wR2 = 0.0777
R indices (all data)	R1 = 0.0261, wR2 = 0.0653	R1 = 0.0286, wR2 = 0.0790
Δρ (e.Å^{-3})	2.629 and -2.274	1.205 and -1.414

Of course, it is worth mentioning the previous reports on this tungstate that are an old and poor-quality single-crystal refinement to R = 11% from Weissenberg photographs [4], and a more recent and much better refinement to Rp = 6% from powder data [5]. To facilitate the comparison with these earlier data, we report here the structure of $LiYbW_2O_8$ in the "nearly orthogonal" *P*2/*n* cell (β ~ 93 °) even if the refinement can be perfectly achieved in the standard *P*2/*c* space group, without any abnormal behavior of the refined parameters. The atomic coordinates and equivalent isotropic displacement parameters are given in Table 2 and the main interatomic distances and angles in Table 3. The crystallographic information file is freely available at the Cambridge Crystallographic Data Center [17] with the CSD number 2086021.

Table 2. Atomic coordinates and equivalent isotropic displacement parameters (Å^2×10^3) for $LiYbW_2O_8$. U_{eq} is defined as ⅓ of the trace of the orthogonalized U_{ij} tensor.

	Wyckoff position	x	y	z	U_{eq}
Yb	2*f*	¾	0.1948(1)	¼	7(1)
W	4*g*	0.2508(1)	0.3187(1)	0.5157(1)	5(1)
Li	2*e*	¾	0.225(7)	¾	33(8)
O1	4*g*	0.4059(12)	0.1230(11)	0.6340(6)	9(1)
O2	4*g*	-0.4652(12)	0.4111(11)	0.8869(6)	10(1)
O3	4*g*	0.1055(13)	0.1300(12)	0.3886(6)	12(1)
O4	4*g*	0.5532(12)	0.3918(11)	0.4035(6)	7(1)

Table 3. Main bond lengths [Å] and angles [°] in $LiYbW_2O_8$

W–O1	1.775(6)	Yb–O4	2.179(6)	Li–O1	2.09(1)
W–O3	1.787(6)	Yb–O4$^{\#6}$	2.179(6)	Li–O2$^{\#8}$	2.08(2)
W–O2$^{\#1}$	1.845(6)	Yb–O3#7	2.210(6)	Li–O2$^{\#13}$	2.08(2)
W–O4	1.971(6)	Yb–O3$^{\#8}$	2.210(6)	Li–O1$^{\#12}$	2.09(1)
W–O4$^{\#2}$	2.078(6)	Yb–O1$^{\#9}$	2.328(6)	Li–O3$^{\#5}$	2.60(3)
W–O2$^{\#3}$	2.253(6)	Yb–O1$^{\#5}$	2.328(6)	Li–O3^{15}	2.60(3)
W$^{\#1}$–O2–W$^{\#16}$	105.4(3)			W–O2–Yb$^{\#4}$	127.6(4)
W–O4–W$^{\#2}$	108.4(3)	W$^{\#14}$–O2–Yb$^{\#11}$	85.6(2)	W–O4–Yb	132.1(3)
W–O1–Yb$^{\#5}$	133.2(3)	W$^{\#1}$–O2–Yb$^{\#11}$	95.6(2)	W$^{\#2}$–O4–Yb	118.0(3)

Symmetry transformations used to generate equivalent atoms: $^{\#1}$ $-x-½,y,{}^3/_2-z$; $^{\#2}$ $1-x,1-y,1-z$; $^{\#3}$ $x+½,1-y,z-½$; $^{\#4}$ $x-1,y,z$; $^{\#5}$ $1-x,-y,1-z$; $^{\#6}$ ${}^3/_2-x,y,½-z$; $^{\#7}$ $½-x,y,½-z$; $^{\#8}$ $x+1,y,z$; $^{\#9}$ $x+½,-y,z-½$; $^{\#10}$ $x+{}^3/_2,1-y,z-½$; $^{\#11}$ $-x,1-y,1-z$; $^{\#12}$ ${}^3/_2-x,y,{}^3/_2-z$; $^{\#13}$ $½-x,y,{}^3/_2-z$; $^{\#14}$ $x-½,1-y,z+½$; $^{\#15}$ $x+½,-y,z+½$

Anyway, applying the transformation matrix $[1\,0\,0\;\;0\,\bar{1}\,0\;\;\bar{1}\,0\,\bar{1}]$ converts the cell parameters into the "more oblique" standard *P*2/*c* monoclinic lattice of the same volume and parameters $a = 4.991$, $b = 5.796$, $c = 10.813$ Å, $\beta = 114.08$ °. To obtain atom positions in the *P*2/*c* lattice, it is appropriate to simply apply the transformation $[1\,0\,\bar{1}\;\;0\,\bar{1}\,0\;\;0\,0\,\bar{1}]$ to the atomic coordinates.

3.2.2. Structure of the double molybdate $LiYbMo_2O_8$

The diffraction data collected for a colorless diamond-like crystal were indexed in a tetragonal cell of parameters $a = b = 5.1149(1)$, $c = 11.0919(4)$ Å. The extinction conditions seemingly indicate the centrosymmetric $I4_1/a$ space group in which was found and refined an initial structural solution. Therefore, as also pointed out in other works [1, 20], non-negligible X-ray reflections which do not satisfy the extinction conditions of the $I4_1$ and $I4_1/a$ space groups were found. They are only allowed in the non-centrosymmetric $I\bar{4}$ tetragonal symmetry. Very similar agreement R-factors were reached for the least-square refinement in these three space groups, but the best S-factor (goodness of fit) was obtained for the symmetry $I\bar{4}$. In all these

groups, the Li and the Yb atoms share the same crystallographic sites as found in the model described by Volkov et *al*. [1]. Besides, all attempts have failed to resolve this Yb/Li atomic disorder in other space groups of lower symmetry, which corroborates the earlier results [1, 2, 20]. The space group $I\bar{4}$ was thus finally retained for the final refinement leading to R1 = 2.88%. The loss of the inversion center is directly related to a reduction in symmetry with respect to the $I4_1/a$ Scheelite structure type [2].

The most relevant data on the structure of $LiYbMo_2O_8$ are listed in Table 1 while Table 4 gives the positions of atoms and Table 5 the main interatomic distances. More details can be found in the CIF file (CSD number 2086022) freely accessible at CCDC [17].

Table 4. Atomic coordinates and displacement parameters ($Å^2 \times 10^3$) for $LiYbMo_2O_8$.

Wyckoff position		x	y	z	U_{eq}
Li/Yb1	2*b*	½	½	0	7(1)
Li/Yb2	2*c*	0	½	¼	10(1)
Mo3	2*d*	½	0	¼	10(1)
Mo4	2*a*	0	0	0	10(1)
O1	8*g*	0.6579(6)	0.2465(6)	0.1640(4)	18(1)
O2	8*g*	0.1560(6)	0.2488(7)	0.0861(4)	18(1)

Li/Yb ratio: 0.526/0.474(2) at site 2*b* and 0.529/0.471(2) at site 2*c*.

Table 5. Main bond lengths [Å] and angles [°] for $LiYbMo_2O_8$.

Mo3−O1	1.776(4)	Mo4−O2−Yb1	120.2(2)	Yb1−O1	2.375(4)
Mo3−O1$^{\#12}$	1.776(4)	Mo4−O2−Yb2	130.5(2)	Yb1−O1$^{\#1}$	2.375(4)
Mo3−O1$^{\#15}$	1.776(4)			Yb1−O1$^{\#2}$	2.375(4)
Mo3−O1$^{\#14}$	1.776(4)			Yb1−O1$^{\#3}$	2.375(4)
Mo4−O2	1.780(3)			Yb1−O2	2.379(4)
Mo4−O2$^{\#4}$	1.780(3)			Yb1−O2$^{\#1}$	2.379(4)
Mo4−O2$^{\#5}$	1.780(3)			Yb1−O2$^{\#2}$	2.379(4)
Mo4 −O2$^{\#13}$	1.780(3)			Yb1−O2$^{\#3}$	2.379(4)

Mo3−O1−Yb1	130.1(2)	Yb2−O2	2.365(4)
Mo3−O1−Yb2$^{\#6}$	120.4(2)	Yb2−O2$^{\#7}$	2.365(4)
		Yb2−O2$^{\#8}$	2.365(4)
		Yb2−O2$^{\#9}$	2.365(4)
		Yb2−O1$^{\#2}$	2.377(3)
		Yb2−O1$^{\#10}$	2.377(3)
		Yb2−O1$^{\#11}$	2.377(3)
		Yb2−O1$^{\#12}$	2.377(3)
		Yb2−O2−Yb1	105.3(1)
		Yb1−O1−Yb2$^{\#6}$	105.1(1)

Symmetry transformations used to generate equivalent atoms: $^{\#1}$ *y*,1−*x*,−*z* ; $^{\#2}$ 1−*x*,1−*y*,*z* ; $^{\#3}$ 1−*y*,*x*,−*z* ; $^{\#4}$ −*y*,*x*,−*z* ; $^{\#5}$ −*x*,−*y*,*z* ; $^{\#6}$ *x*+1,*y*,*z* ; $^{\#7}$ ½−*y*,½+*x*,½−*z* ;$^{\#8}$ −*x*,1−*y*,*z* ; $^{\#9}$ *y*−½,½−*x*,½−*z* ; $^{\#10}$ *x*−1,*y*,*z* ; $^{\#11}$ *y*−½,−*x*+$^{3}/_{2}$,½−*z* ; $^{\#12}$ ½−*y*,*x*−½,½−*z* ; $^{\#13}$ *y*,−*x*,−*z*; $^{\#14}$ *y*+½,½−*x*,½−*z* ; $^{\#15}$ 1−*x*,−*y*,*z*.

Our results from single-crystal data corroborate the structure previously published from powder data for $LiYbMo_2O_8$ [1], confirming the space group $I\bar{4}$, and bringing a slight improvement in the agreement factors. Also, our results give better accuracy on the interatomic distances showing a more regular arrangement of oxygen around both the Mo and Yb centers.

3.2.3. Atomic arrangements in the $LiYbX_2O_8$ family

As already noticed in ternary metal oxides AXO_4 with X = W^{VI} or Mo^{VI}, double oxides of general formula ATX_2O_8 with T = rare earth element, are also known to belong to the parent family of a structure either Scheelite or Wolframite, depending on the ionic radius of the *A* monovalent element [2, 4-6]. In the tetragonal Scheelite structure-type (which prototype is $CaWO_4$), the oxygen atoms are arranged in coordination 8 around the *A* and *T* atoms and, in coordination 4 around the *X* atoms. By contrast, a nearly hexagonal arrangement of the oxygen atoms is found in the structure of Wolframite (the most common iron-manganese

tungsten oxide mineral between the extreme composition limits $MnWO_4$ and $FeWO_4$) where all the atoms are 6-fold coordinated by oxygen.

The crystal structure of the double molybdate $LiYbMo_2O_8$ derives from the Scheelite-type with an atomic local disorder at cations sites as Li^+ and Yb^{3+} cations share their sites. It is built up with regular MoO_4 tetrahedra involving Mo–O distances of ~1.78 Å (Table 5) and MO_8 dodeca-deltahedra (M = Li/Yb) characterized by M–O distances from 2.366 to 2.379 Å. The MO_8 polyhedra are centered on M atoms, *i.e.* either on Yb or Li which are distributed randomly on the same 2*b* and 2*d* positions according to the respective Yb/Li contents refined to 0.474/0.526(2) and 0.529/0.471(2). The MO_8 polyhedron shares each of its vertices with a MoO_4 regular tetrahedron and, additionally, two of its edges with two neighboring MO_8 units as seen in Figure 1 which gives a representation of the polyhedral packing in the unit cell.

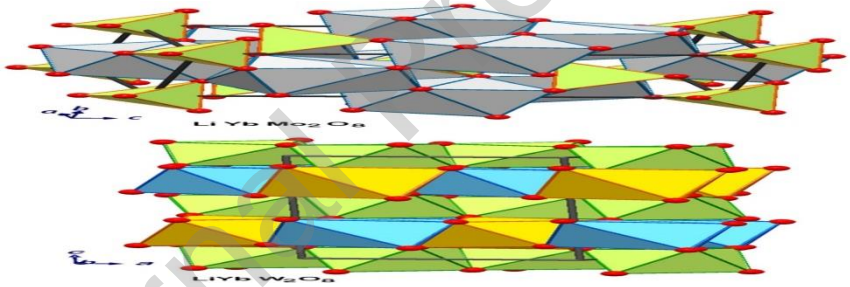

Figure 1. Polyhedral packing in –*up*– tetragonal $LiYbMo_2O_8$ with MoO_4 tetrahedra (green) and Yb/Li centered MO_8 dodeca-deltahedra (grey); –*down*– monoclinic $LiYbW_2O_8$ with octahedra WO_6 (green), YbO_6 (orange), and LiO_6 (blue). Unit cells are drawn as grey lines.

Instead, the double tungstate $LiYbW_2O_8$ adopts a Wolframite-type structure in which each W, Yb, and Li atom is coordinated by six oxygen atoms leading to more or less distorted octahedra packed within the unit cell, Figure 1 and Table 3. It is classified as an ordered crystal as both Li^+ and Yb^{3+} occupy individual sites [2]. With bond lengths varying at most 0.07 Å from the mean Yb–O distance of 2.24 Å, the smallest distortion is observed around the largest Yb atom. Then, deviations around W and Li are 0.188 and 0.27 Å from the average

bond lengths of 1.95 and 2.26Å. The Wolframite-type structure of the tungstate can be described as alternating two kinds of parallel layers. The first one, at z ~ ¼, ¾, is composed of regular YbO_6 octahedra (Yb–O distances ranging from 2.179 to 2.328 Å) and LiO_6 distorted octahedra (Li–O distances from 2.079 to 2.596 Å). The second, at z ~ 0, ½, consists of WO_6 distorted octahedra with W–O distances ranging from 1.774 to 2.253 Å forming "zig-zag chains" *via* edge-sharing (see below).

3.2.4. Polyhedra and connection types in the $LiYbX_2O_8$ compounds

Now, paying special attention to the distribution of the *X* atoms (*X* = W, Mo) in the two structures, some interesting structural differences emerge. The arrangement in $LiYbMo_2O_8$ is such that the Mo atoms, distant by 3.772 Å, are "interconnected" through Mo–{O_2}–Mo asymmetric double bridges (2 × Mo–O–Mo bridges) established with Mo–O distances of ~1.78 and ~2.83 Å as drawn in Figure 2.

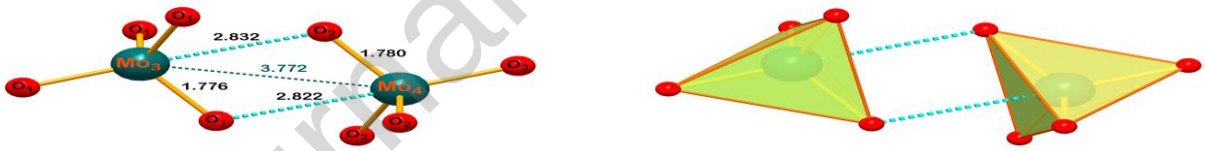

Figure 2. Representation of the MoO_4 tetrahedra and their interconnection mode *via* Mo–{O_2}–Mo double bridges. Interatomic distances are given in Å on the left drawing.

However, the longest distances Mo4–O1 of 2.822(4) and Mo3–O2 2.832(4) Å do not correspond to "true" covalent bonds because much greater than the sum of the covalent radii of the elements, which is ~ 2.2 Å [18], but they could be seen as long-distance interactions. This is one of the reasons why a description in terms of isolated MoO_4 tetrahedra is preferable here.

Instead, each W atom in $LiYbW_2O_8$ is distant by 3.2695(5) and 3.2854(5) Å from its two closest tungsten neighbors. As represented in Figure 3, tungsten atoms are "interconnected" through oxygen atoms involved in asymmetric W–{O_2}–W double bridges.

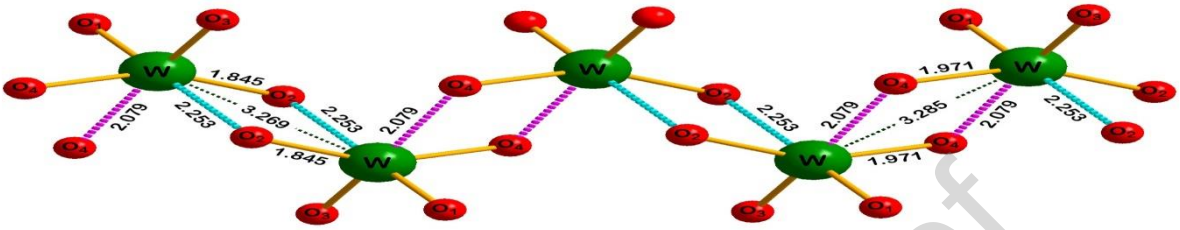

Figure 3. Regular alternation of W–{O2}–W asymmetric double bridges of two types defining two kinds of W_2O_{10} "dimeric units" associated in infinite $^{\infty}_{1}[WO_4]$ "zig-zag chains" aligned with the *a*-axis. The interatomic distances are given in Å in the drawing.

With W-O bonds of 1.971 and 2.079 Å, the double bridge established with the atom O4 (right part in Figure 3) is a little more symmetric than the one built with the atom O2 (left part in Figure 3) with W-O bonds of 1.845 and 2.253 Å. Even the longest W–O distance of 2.253 Å remains slightly shorter than 2.28 Å, the sum of the covalent radii of the elements, indicating a covalent bonding interaction. Thus, two types of W_2O_{10} "dimeric units" must be considered in this structural arrangement either formed of W–{O_2}–W double bridges established with O2 or O4 atoms, as illustrated in Figure 3. In that case, a better description of the structure would be provided by the use of dimeric units. Nevertheless, the sequence of double bridges W–{O_2}–W established through O2 atoms alternating with double bridges W–{O_2}–W established through O4 atoms rather supports a structural description in terms of polymeric units. Another alternative would be to describe the structure using WO_6 octahedra, each of which shares an edge with two alike units to form infinite zig-zag chains $^{\infty}_{1}[WO_4]$ oriented in the direction of the *a*-axis, Figure 4.

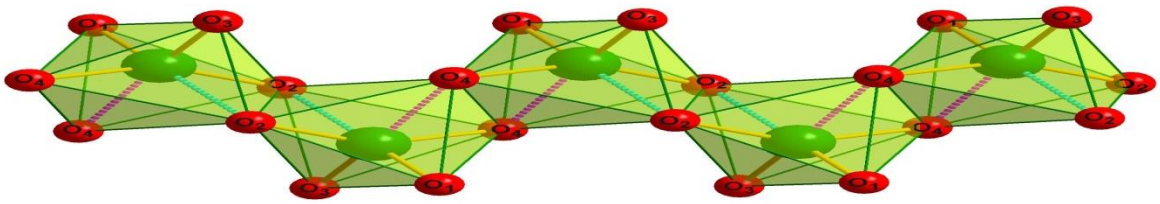

Figure 4. The infinite $^{\infty}_{1}[WO_4]$ zig-zag chains viewed as a series of edge-sharing WO_6 units.

It should be stressed that the existence of such zig-zag chains extended infinitely along the [001] direction has already been reported earlier in the monoclinic structure of the tungstate $NaIn(WO_4)_2$ described in the *P*2/*c* symmetry [21].

3.2.5. Structural evolution in the $AYbX_2O_8$ family

On a more general aspect, it is interesting to notice a structural evolution within the $AYbX_2O_8$ family with the nature of the *A* and *X* elements (*A* = Li, K and *X* = Mo, W). As seen above, the tetragonal structure of the lithium ytterbium double molybdate would be better described with isolated MoO_4 tetrahedra and $(Yb/Li)O_8$ distorted (square antiprism) polyhedra and therefore the formulation $LiYb(MoO_4)_2$ would be more suitable.

When tungsten replaces molybdenum at position *X* in the $LiYbX_2O_8$ family, significant changes occur in the structural arrangement that undergoes a complete reorganization including, in particular, an orderly distribution of the Yb and Li atoms. The global symmetry is lowered from tetragonal to monoclinic and the local environment of atoms changes so that W, Yb, and Li are all 6-coordinated. Therefore, the absence of individualized tetrahedra in this tungstate further justifies the formulation $LiYbW_2O_8$ rather than $LiYb(WO_4)_2$.

When lithium is replaced by a larger alkali metal, hereby K, at the *A* position in the ytterbium double molybdate $AYbMo_2O_8$, the symmetry of the structure evolves from tetragonal to orthorhombic. An ordered atomic distribution is still observed in the potassium molybdate where isolated MoO_4 tetrahedral units are preserved which agrees with the formulation

$KYb(MoO_4)_2$ [12]. Likewise, the Yb atoms retain eight oxygen neighbors in the potassium molybdate, forming square antiprisms YbO_8. On the contrary, the LiO_8 units of symmetry $\overline{4}$ in the lithium molybdate are replaced in $KYbMo_2O_8$ by highly distorted octahedral units KO_6, with the symmetry C_2, built around the potassium atoms [12].

3.3 Vibrational study

The room-temperature Raman spectra of the investigated materials were registered in atmospheric pressure in the wavenumber range 70–1000 cm^{-1}. Their general aspect differs from one to the other, but both of them do not present vibrational features beyond 1000 cm^{-1}, Figure 5. The presence of a higher number of vibrational bands in the Yb-stoichiometric crystal $LiYbW_2O_8$ compared to $LiYbMo_2O_8$ is an indication of an increase in the coordination number of the *d*-elements from four to six, as shown in the structural part of this work [19]. All Raman active modes in both polymorphs are assigned based on the literature reports.

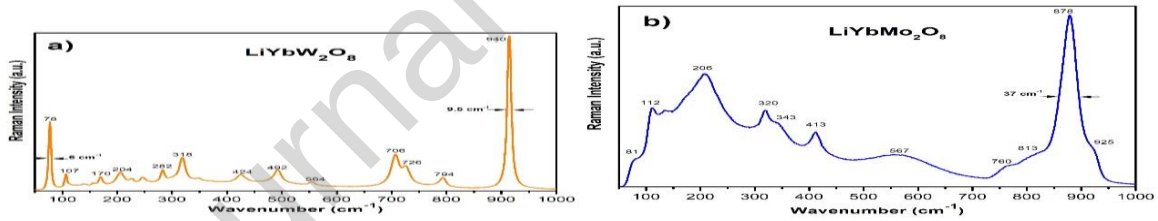

Figure 5. Unpolarized Raman spectra registered at room temperature with $\lambda_{exc} = 473$ nm for the $LiYbX_2O_8$ samples. *X* = W (a); *X* = Mo (b).

The spectral lines are relatively narrow for the new ordered $LiYbW_2O_8$ material containing distorted WO_6 units, Figure 5a, with full-width at half-maximum (FWHM) equal to 6 and 9.5 cm^{-1} for the two main peaks centered at 78 and 940 cm^{-1}, respectively. The well-resolved sharp peaks indicate a high crystalline state for the synthesized material. The most shifted Raman line is located at 940 cm^{-1} and corresponds to the symmetric stretching of the W-O distances of the W-based polyhedra [23]. The Raman spectrum is interpreted in terms of

internal and external modes of the distorted WO_6 octahedra. The internal modes correspond to vibrations of O atoms against W and the external modes imply the movement of WO_6 octahedra as rigid units. The internal asymmetric and symmetric stretching modes of the oxygen atoms forming the distorted WO_6 octahedra are identified in the 700-950 cm^{-1} frequency range. Several weak-intensity lines observed in the domain 450 – 700 cm^{-1} are due to the vibrational modes of the W–{O_2}–W double oxygen bridges in the W_2O_{10} "dimers" associated in infinite zig-zag chains and giving a polymeric feature to the structure of the tungstate, see Figure 3. The frequency range from 250 to 450 cm^{-1} corresponds to the internal bending modes of W-O bonds, while the bending vibrations of the W–{O_2}–W double oxygen bridges, as well as the translation of the Yb^{3+} cations, are expected in 150-250 cm^{-1} frequency range [22-24].

The lithium ytterbium oxo-molybdate crystallizes in the space group S_4^2-$I\overline{4}$ and contains isolated regular tetrahedra MoO_4^{2-}. Its room temperature (300K) Raman spectrum is given in Figure 5b. The FWHM is equal to 37 cm^{-1} for the main peak centered at 878 cm^{-1} and bandwidths are larger than those observed for the ordered $LiYbW_2O_8$ double tungstate, Figure 5a. This could be explained by the existence in the $LiYbMo_2O_8$ crystal structure of two cationic positions occupied by both Li^+ and Yb^{3+} cations, each with a 50% occupancy factor, and two crystallographically distinguishable Mo^{6+} cations [2, 22, 25]. The Raman bands in the frequency range 740-900 cm^{-1} are attributed to the internal asymmetric and symmetric stretching vibrations of the M-O bonds in the regular MoO_4 tetrahedra while the symmetric and asymmetric bending modes δ(OMoO) are found in the 280-450 cm^{-1} range [25, 26]. The translational and rotational vibrations of the MoO_4 tetrahedra are expected at wavenumbers lower than 260 cm^{-1} with the external vibrations involving the Yb/Li-centered polyhedra [27].

It is to be noticed that the 300 K Raman spectrum of $LiYbMo_2O_8$ published by Volkov et *al.* [1] shows a close resemblance to ours, although, unlike our spectrum, it has several small

bands beyond 1000 cm^{-1}, the origin of which is not discussed. Their Raman spectra also exhibit a large feature from 500 to 700 cm^{-1} as in our vibrational spectrum, Figure 5b, which is not discussed as its origin is not clear.

3.4 Magnetic properties

The results of the susceptibility measurements with a weak external magnetic field of *H* =1000 Oe in the temperature range from 1.8 to 300 K are illustrated in Figure 6**.** The temperature dependence of the inverse susceptibility (1/χ) for the two samples under study have been fitted in the paramagnetic region (temperature range 55-300 K) with a Curie–Weiss law $\chi = C/(T - \theta_{CW})$, where *C* and θ_{CW} are constants, Figure 6.

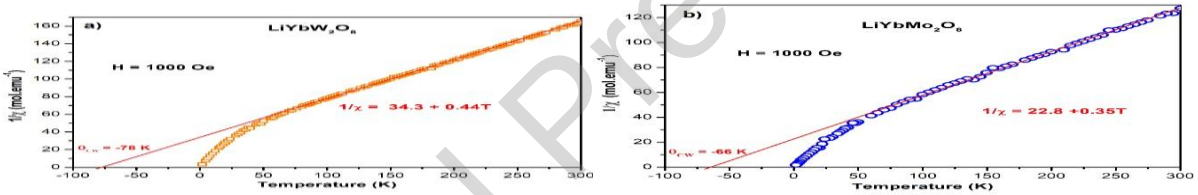

Figure 6. Inverse susceptibility 1/χ *vs.* temperature curves for the samples $LiYbX_2O_8$ in a constant applied magnetic field *H* showing a Curie-Weiss behavior (red line) at high temperatures. *X* = W (a); *X* = Mo (b).

The least-squares parameters used in the curve fitting are gathered in Table 6 where *C* is the Curie-Weiss constant, θ_{CW} the paramagnetic Curie-Weiss temperature, and μ_{eff} the effective magnetic moment. The experimental effective magnetic moments are calculated from the Curie constant according to the formula $\mu_{eff} = (8 \times C)^{1/2}$.

Table 6. Least-squares parameters from the inverse susceptibility curves fit (50-300 K)

	C (emu.K.mol^{-1})	θ_{CW} (K)	μeff (μB/Yb-atom)
$LiYbW_2O_8$	2.27	−78	4.26
$LiYbMo_2O_8$	2.86	−66	4.78

The experimental effective magnetic moments found for both $LiYbW_2O_8$ and $LiYb_2MoO_8$ are in good agreement with the theoretical value of μ_{eff} expected for the Yb^{3+} free-ion. Indeed, the electronic configuration of the isolated paramagnetic Yb^{3+} ion is $[Xe]\ 4f^{13}$ with $[Xe] = 2s^2 2p^6 3s^2 3p^6 3d^{10} 4s^2 4p^6 4d^{10}$, which yields the spectral term $^2F_{7/2}$ as the ground state, and an effective magnetic moment μ_{eff} of 4.50 μ_B/ Yb^{3+}. The result of the Curie–Weiss fit in the temperature range 55-300 K confirms that the Yb chemical element is only present as Yb^{3+} ion in the two structures.

The large negative values obtained for θ_{CW} for the tungstate and molybdate crystals, Table 6, may suggest that the two polycrystalline samples present an antiferromagnetic coupling. Such large negative values of θ_{CW} have already been reported for the double molybdate $KYb(MoO_4)_2$ described in the orthorhombic space group *Pbcn*, and for other Yb-containing oxide materials [12, 29, 30].

In the 1.8-50 K temperature range and for H = 1000 Oe, the inverse susceptibility data of the two materials no longer follow a strict linear behavior with temperature and do not present an anomaly, Figure 6. The tails below 55 K could correspond to paramagnetic tails that arise when some isolated regions in a material present imperfections in the antiferromagnetic ordering [28], or be due to a crystal field effect on the $^2F_{7/2}$ ground state of Yb^{3+} [29].

The first magnetization M curves registered at several temperatures from 300 to 1.8 K as a function of the applied magnetic field H ranging from 0 to 50 kOe are presented in Figure 7.

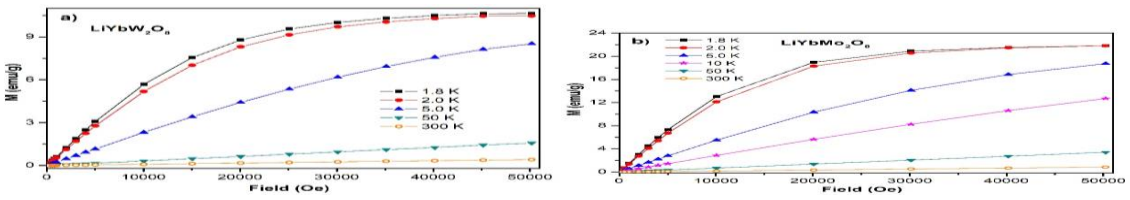

Figure 7. Magnetization M-H curves at various temperatures for $LiYbW_2O_8$ (a) and $LiYbMo_2O_8$ (b).

For temperatures comprised between 50 and 300 K, the M-H plots recorded for the two samples under study are linear with a weak magnetization M in agreement with a paramagnetic behavior. For the selected temperatures in the range $1.8 \leq T < 50$ K, the magnetization M strongly depends on the external magnetic field and, for T = 1.8 and 2 K, it displays a tendency to saturation which could be related to a potential antiferromagnetic coupling [28]. Similar behaviors were already observed for the $KYb(MoO_4)_2$ material [12].

The evolution of the magnetic properties measured for the tetragonal $LiYbMo_2O_8$ and the monoclinic $LiYbW_2O_8$ are very similar and are not dependent on their room-temperature crystal structure.

4. CONCLUSION

The current work reports the results of an X-ray diffraction study of single crystals of an oxo-tungstate and an oxo-molybdate based on lanthanide Yb^{3+} and alkali Li^{+} cations, both compounds being obtained by the high-temperature flux technique in the form of crystals of sub-millimeter size grown spontaneously. The structural results confirm the disordered Yb/Li arrangement for the molybdate $LiYbMo_2O_8$, derived from the tetragonal Scheelite-type structure, and the ordered Wolframite-like arrangement for the tungstate monoclinic structure of $LiYbW_2O_8$. Raman investigation at room temperature supports the presence of isolated MoO_4^{2-} tetrahedra in $LiYbMo_2O_8$, and the existence in $LiYbW_2O_8$ of WO_6 octahedra, joined by W–{O_2}–W double oxygen bridges in polymeric units.

Susceptibility is studied as a function of temperature from 1.8 to 300 K. The inverse susceptibility curves follow a Curie–Weiss law in the 50-300 K region with a very large negative paramagnetic constant θ_{CW} of −78 K for $LiYbW_2O_8$ (−66 K for $LiYbMo_2O_8$). The origin of these large negative values of θ_{CW} could be explained by the existence of an antiferromagnetic coupling under 50 K, in agreement with the evolution of the shapes of the

M-H curves recorded at various temperatures in the range of 1.8-300 K. The existence of long-range antiferromagnetic order of the Yb^{3+} ions is not demonstrated. Further physical experiments and investigations would be necessary to better understand the magnetic properties of the $LiYbW_2O_8$ and $LiYbMo_2O_8$ materials.

Acknowledgments

Raman and magnetic measurements were done at the Platform of Analysis and Characterization (PAC) of the Pôle Chimie Balard in Montpellier, France. The single-crystal X-ray diffraction experiments were done using the technological resources of the X-ray and gamma-ray network of the University of Montpellier, France.

Funding: This work was supported by the French Ministry of Higher Education, Scientific Research and Innovation, and the French National Center of Scientific Research (CNRS).

REFERENCES

[1] Growth, structure, and evaluation of laser properties of $LiYb(MoO_4)_2$ single crystal.

V. Volkov, C. Cascales, A. Kling, C. Zaldo

Chem. Mater. 17 (2005) 291-300.

10.1021/cm049095k

[2] The optical spectroscopy of lanthanides R^{3+} in $ABi(XO_4)_2$ (A = Li, Na; X = Mo, W) and $LiYb(MoO_4)_2$ multifunctional single crystals: Relationship with the structural local disorder.

C. Cascales, A. Méndez Blas, M. Rico, V.Volkov, C. Zaldo

Opt. Mater. 27 (2005) 1672-1680.

10.1016/j.optmat.2004.11.051

[3] Polymorphism of the double molybdates and tungstates of mono- and trivalent metals with the compositions $M^+R^{3+}(EO_4)_2$

P. V. Klevtsov, R.F. Klevtsova

J. Struct. Chem. 18 (1977) 339-355.

10.1007/BF00753083

[4] Variations on a single wolframite motif in the structures of $LiYb(WO_4)_2$, $LiFe(WO_4)_2$, and $NaFe(WO_4)_2$

R.F. Klevtsova, N.V. Belov

Sov. Phys. Crystallogr. 15 (1970) 32-35 (Kristallografiya 15 (1970) 43-46).

[5] Crystal structure of $LiLnW_2O_8$ (Ln = lanthanides and Y): An X-ray powder diffraction study

J.M. Postema, W.T. Fu, D.J.W. Ijdo

J. Solid State Chem. 184 (2011) 2004-2008.

10.1016/j.jssc.2011.05.046

[6] Structure and luminescent properties of three new silver lanthanide molybdates.

F. Shi, J. Meng, Y. Ren

J. Solid State Chem. 121 (1996) 236-239.

10.1006/jssc.1996.0033

[7] Electrochemical characterization of amorphous $LiFe(WO_4)_2$ thin films as positive electrodes for rechargeable lithium batteries.

C.-L. Li, Z.-W Fu

Electrochim. Acta 53 (2008) 6434−6443.

10.1016/j.electacta.2008.04.063

[8]. $LiFe(MoO_4)_2$ as a novel anode material for Lithium-Ion Batteries.

N. Chen, Y. Yao, D. Wang, Y. Wei, X. Bie, C. Wang, G. Chen, F. Du

ACS Appl. Mater. Interfaces 6 (2014) 10661−10666.

10.1021/am502352c

[9] Ferroelastic domain structure in trigonal double molybdates and tungstates

Wl. Zapart, M. Zapart

In book: Solid State Physics in Modern Materials Research Chapter: 9

Publisher: Czestochowa University of Technology, Faculty of Materials Processing Technology and Applied Physics, March 2010.

Editors: K.Dziliński, J.Wysłocki

[10] Antiferromagnetism of double molybdate $LiFe(MoO_4)_2$

M. Liu, Y. Zhang, T. Zou, V. Ovidiu Garlea, T. Charlton, Y. Wang, F. Liu, Y. Xie, X. Li, L. Yang, B. Li, X. Wang, S. Dong, J.-M. Liu

Inorg. Chem. 59 (2020) 8127–8133.

10.1021/acs.inorgchem.0c00432

[11] Cycloidal magnetism driven ferroelectricity in double tungstate $LiFe(WO_4)_2$

M. Liu, L. Lin, Y. Zhang, S. Li, Q. Huang, V. O. Garlea, T. Zou, Y. Xie, Y. Wang, C. Lu, L. Yang, Zhibo Yan, Xiuzhang Wang, Shuai Dong, J. Liu less

Phys. Rev. B (2017) 195134.

10.1103/PhysRevB.95.195134

[12] Growth, single-crystal structure, and magnetic properties of the double molybdate $KYb(MoO_4)_2$

P. Armand, C. Reibel, D. Granier, M. Tillard

J. Phys. Chem. Solids 154 (2021) 110023.

10.1016/j.jpcs.2021.110023.

[13] Bruker, APEX3. Version 2017.3-0, Bruker AXS, Inc., Madison, Wisconsin, USA, 2017

[14] CrysAlis'Red' 171 software package,

Oxford Diffraction Ltd, Abingdon, United Kingdom, (2004).

[15] Crystal structure refinement with SHELXL

G. M. Sheldrick

Acta Crystallogr. C71 (2015) 3-8

10.1107/S2053229614024218

[16] SHELXT - Integrated space-group and crystal-structure determination

G. M. Sheldrick

Acta Crystallogr. A71 (2015) 3-8

10.1107/S2053273314026370

[17] http://www.ccdc.cam.ac.uk/conts/retrieving.html (or from the CCDC, 12 Union Road, Cambridge CB2 1EZ, UK; Fax: +44 1223 336033; E-mail: deposit@ccdc.cam.ac.uk).

[18] Covalent Radii. (2020, November 3). Retrieved March 30, 2021, from https://chem.libretexts.org/@go/page/2182

[19] In Situ Neutron Diffraction Studies of $LiCe(WO_4)_2$ Polymorphs: Phase Transition and Structure−Property Correlation

Archana K. Munirathnappa, Debasmita Dwibedi, James Hester, Prabeer Barpanda, Diptikanta Swain, Chandrabhas Narayana, Nalini G. Sundaram

J. Phys. Chem. C 123 (2019) 1041−1049.

10.1021/acs.jpcc.8b09364

[20] Double tungstate and molybdate crystals for laser and nonlinear optical applications

E.V. Zharikov, C. Zaldo, F. Diaz

MRS bulletin 34 (2009) 271-276.

10.1557/mrs2009.78

[21] Single-crystal synthesis and investigation of the double tungstates $NaR^{3+}(WO_4)_2$ where R^{3+}= Fe, Sc, Ga and In.

P. V. Klevtsov, R.F. Klevtsova

J. Solid State Chem. 2 (1970) 278-282.

[22] Optical spectroscopy of Dy^{3+} ions doped in $KY(WO_4)_2$ crystals

L. Macalik, J. Hanuza, B. Macalik, W. Ryba-Romanowski, S. Golab, A. Pietraszko

J. Luminescence 79 (1998) 9-19.

10.1016/S0022-2313(98)00020-9

[23] Non-stoichiometric $KY(WO_4)_2$: crystal growth, chemical and physical characterization

E.Galluccia, C.Goutaudiera, G.Boulona, M.Th.Cohen-Adada, B.F.Mentzen

J. Crystal Growth 209 (2000) 895-905.

10.1016/S0022-0248(99)00623-5

[24] The Incorporation of Li^+ Cations in Yttrium Tungstate and Silicate Tungstate

K. V. Dorn, T. Schustereit, S. Strobel, I. Hartenbach

Z. Anorg. Allg. Chem. 643 (2017) 2050-2056.

10.1002/zaac.201700305

[25] Structure and Vibrational Properties of Tetragonal Scheelite $NaBi(MoO_4)_2$

J. Hanuza, A. Haznar, M. Maczka, A. Pietraszko, A. Lemiec, J. H. van der Maas, E. T. G. Lutz

J. Raman Spectrosc 28 (1997) 953-963.

[26] Triple molybdate scheelite-type upconversionphosphor $NaCaLa(MoO_4)_3:Er^{3+}/Yb^{3+}$: structuraland spectroscopic properties

Chang Sung Lim, Aleksandr S. Aleksandrovsky, Maxim S. Molokeev, Aleksandr S. Oreshonkov, Denis A. Ikonnikovg, Victor V. Atuchin

Dalton Trans. 45 (2016) 15541.

10.1039/c6dt02378a

[27] Electronic structure, growth mechanism and photoluminescence of $CaWO_4$ crystals

L. S. Cavalcante, V. M. Longo, J. C. Sczancoski, M. A. P. Almeida, A. A. Batista, J. A. Varela, M. O. Orlandi, E. Longo, M. Siu Lic

CrystEngComm. 14 (2012) 853

10.1039/c1ce05977g

[28] Crystal structure and magnetic properties of $Sr_2Ni_{1-x}Mg_xMoO_6$ ($x = 0$, 0.25, 0.5, and 0.75) polycrystals

N. Urusova, M. Rajesh Kumar, M. Semkin, E. Filonova,, M. Kratochvilova, D. Neznakhin, K. Grzhegorzhevskii, A. Ostroushko, J.-G. Park, A. Pirogov

Solid State Sci. 99, 2020, 106008

10.1016/j.solidstatesciences.2019.106008

[29] Structural and magnetic study of Yb^{3+} in the perovskites Sr_2YbMO_6 (M=Nb, Ta, Sb)

F. C. Coomer, J. Campbell, N. Giordano, O. M.Collins, E. J.Cussen

J. Solid State Chem. 221 (2015) 411- 417.

10.1016/j.jssc.2014.10.025

[30] Crystal growth, crystal structure, and anisotropic magnetic properties of $KBaR(BO_3)_2$ (R = Y, Gd, Tb, Dy, Ho, Tm, Yb, and Lu) triangular lattice materials

S. Guo, T. Kong, F. Alex Cevallos, K. Stolze, R. J. Cava

J. Magn. Magn. Mater. 472 (2019) 104-110

10.1016/j.jmmm.2018.10.037

Declaration of interests

☒ The authors declare that they have no known competing financial interests or personal relationships that could have appeared to influence the work reported in this paper.

☐The authors declare the following financial interests/personal relationships which may be considered as potential competing interests:

Structure, vibrational and magnetic characteristics of $LiYbX_2O_8$ (X = W, Mo) single-crystals

P. Armand, D. Granier, C. Reibel, L. Daenens, M. Tillard

ICGM, Univ. Montpellier, CNRS, ENSCM, Montpellier, France

Highlights

Flux-growth of sub-millimeter size and colorless $LiYb(XO_4)_2$ (X= Mo^{VI}, W^{VI}) crystals.

Ordered distribution of Li^+ and Yb^{3+} in $LiYbW_2O_8$ ($P2/n$) and W–{O_2}–W double oxygen bridges.

Crystallization of $LiYbMo_2O_8$ in tetragonal symmetry ($I\bar{4}$) with isolated MoO_4^{2-} anions.

Disordered distribution of the Li^+ and Yb^{3+} ions in $LiYbMo_2O_8$ crystal structure

Very large negative values of the θ_{CW} Weiss constants.

M-H curve shape evolution with the temperature in favor of antiferromagnetic coupling in both structure.